



# Tracking the effect of binder length on colloidal stability and bioconjugation of gold nanoparticles

J. P. Oliveira<sup>1</sup> · W. J. Keijok<sup>1</sup> · A. R. Prado<sup>2</sup> · M. C. C. Guimarães<sup>1</sup>

Received: 30 May 2018 / Accepted: 11 July 2018 / Published online: 20 July 2018  
© Springer-Verlag GmbH Germany, part of Springer Nature 2018

## Abstract

Understanding the organization of self-assembled monolayers (SAMs) on gold nanoparticles (AuNPs) as protective coatings is a key role of biological applications of nanomaterials. Here, we report the influence on the stability of the surface coverage of three mercaptocarboxylic ligands onto AuNPs, mercaptopropanoic acid (MPA), mercaptoundecanoic acid (MUA) and mercaptopropionic acid (MHA) under different conditions. In addition, we optimized a bioconjugation route using bovine serum protein (BSA) as a protein model. AuNPs and successful binding of ligands and BSA on the AuNPs were analyzed by UV–Vis, TEM, FTIR, RAMAN, DLS and zeta potential. The size of as-synthesized AuNPs was  $18 \pm 1.2$  nm with surface plasmon resonance (SPR) peak at 522 nm. The magnitude of the bathochromic shift of AuNPs with MPA, MUA and MHA was determined by UV–Vis and the SPR band position of AuNP shifts to 1.5, 3 and 5 nm longer. Moreover, the data show the influence of chain length on colloidal stability and covalent and non-covalent coupling steps with nanomaterials. We demonstrate a method for quantitative determination of the coatings on gold nanoparticles and open new perspectives in understanding the influence of monolayer thickness on the generation of nanobioconjugates for biological applications.

**Keywords** Gold nanoparticles · Colloidal stability · Thiol ligands · Bioconjugation

## Introduction

Nanobioconjugates have been explored by a multitude of applications (Zargar and Hatamie 2013; Terentyuk et al. 2009; Zhou et al. 2014; Peng et al. 2009; Stuchinskaya et al. 2011; Jain et al. 2007; Sperling et al. 2008; El-Sayed 2004; Schroeder et al. 2012; Saha et al. 2012), such as platforms for diagnostic technologies and next generation therapies (Arruebo et al. 2009). Various nanobioconjugates have been synthesized, proteins are one of the most important classes of biological agents used to be combined with nanomaterials and have been widely applied as a model, since their

structural characteristics provide a number of options for modification and conjugation. Thus, understanding biophysicochemical interactions at the nano–bio interface and how nanoparticles (NPs) interact in biological systems are crucial (Lacerda et al. 2010; Lynch and Dawson 2008).

Studies have shown that the binder length determines the interfacial properties (Levy et al. 2006; MacCuspie et al. 2011), such as nanoparticles (NPs) interaction with cell membranes (Bartczak and Kanaras 2011; Sukhanova et al. 2012; Wilson et al. 2004), solubility and molecular recognition (Pease et al. 2007; Tsai et al. 2008). Modified surface NPs are generally known as self-assembly monolayers (SAM's) (Silvia et al. 2000). Although many authors have reported the SAM's, few investigations have included a biological approach, taking into account the stability at different pH conditions, ionic strength and the influence of the ligand chain length on the bioconjugation.

Protein conjugation by electrostatic interaction that presents several deficiencies such as the need for high protein concentrations, random orientation, denaturation and poor reproducibility (Silvia et al. 2000; Kumar 2008; Gole and Murphy 2008). For biological applications, covalent coupling has the advantage of maintaining the tertiary structure

**Electronic supplementary material** The online version of this article (<https://doi.org/10.1007/s13204-018-0843-4>) contains supplementary material, which is available to authorized users.

✉ M. C. C. Guimarães  
marco.guimaraes@ufes.br

<sup>1</sup> Federal University of Espírito Santo, Av Marechal Campos 1468, Vitória, ES 29040-090, Brazil

<sup>2</sup> Federal Institute of Espírito Santo, km 6.5 ES 010, Serra, ES 29173-087, Brazil

of the protein and minimizing possible injuries (Silvia et al. 2000; Thobhani et al. 2010). Therefore, the use of SAM's (covalent coupling) has been the most used strategy. The most commonly used method involves the zero-crosslinking agent, EDC (1-ethyl-3-(3-dimethylaminopropyl) carbodiimide) and NHS (N-hydroxysuccinamide) for the formation of amide bond between carboxyl groups of the linkers and the primary amines of the proteins (25). Although this approach be used in a large number of works, most authors do not discuss how to make the method more efficient (Levy et al. 2006; Bartczak and Kanaras 2011; Sukhanova et al. 2012; Wilson et al. 2004, 25).

Herein we investigated the influence of monolayer thickness on colloidal stability (pH and ionic strength) and bioconjugation efficiency using bovine serum protein (BSA) as a model. The EDC/NHS molar ratio in the covalent coupling was evaluated to establish the best experimental condition for bioconjugation. Finally, we demonstrate a direct influence of binder length on colloidal stability and consequently on bioconjugation.

## Experimental

### Chemicals

Tetrachloroauric acid (G4022) and trisodium citrate (PHR1416), mercaptohexadecanoic acid (448303), 11-mercaptoundecanoic acid (447528), mercaptopropionic acid (M5801), N-hydroxysuccinamide (NHS) (130672), 1-ethyl-3-(3-dimethylaminopropyl) carbodiimide (EDC) (E6383) and lyophilized bovine serum protein (BSA) (05470) were purchased from Sigma-Aldrich. All of the chemicals have analytical purity and were used as received. All the glassware used here were clean with aqua regia solution (3:1 HNO<sub>3</sub> HCl).

### Instruments

Optical properties were evaluated by UV–Vis spectrophotometry (FEMTO 800 XI). The size and morphology of gold nanoparticles were examined by transmission electron microscopy (TEM) operated at 120KV with LaB6 filament (JEM-1400, JEOL Inc.). The crystalline nature of AuNPs was confirmed by X-ray diffractometry (XRD) (D8-ADVANCE, BRUKER-AXS). The total concentration of nanoparticles was determined using plasma inductively coupled to a Perkin Elmer mass spectrometer (ICP-MS) (Optima 7000). The functionalization was investigated by the absorption in the infrared region (FT-MIR FTLA 2000 Bomem) and Raman spectrometry (ALPHA 300R). The Varioskan Flash Fluorescence Detector (Thermo Scientific) was used to determine the total proteins (excitation at

280 nm and with emission scanning from 300 to 500 nm). The MiniSpin (Eppendorf) was used to centrifugation. Ultrapure water for all tests was obtained by the EASYpure II® Thermo Scientific ultrapurification system.

### Softwares

The UV–Vis, IR and Raman graphs as well as for statistical analysis were performed by Origin Pro 8.5 (trial version) and GraphPad Prism version 6.01. Chemical structures were drawn using Chemdraw Prime software (courtesy Perkin Elmer). Image J to quantify the aspect ratio.

### Synthesis and characterization of AUNPs

The synthesis was performed using 15 mL of  $2.5 \times 10^{-4}$  M HAuCl<sub>4</sub> with 1% sodium citrate under stirring for 15 min at 100 °C (Oliveira et al. 2017). Thus, the colloid was cooled in an ice bath and then centrifuged followed by three washes to remove the unreacted substances. The material was then characterized by UV–Vis, TEM, XRD and ICP-MS.

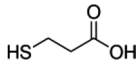
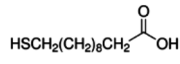
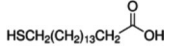
### Surface modification

The thiol ligands used in this study were mercaptopropionic acid (MPA), mercaptoundecanoic acid (MUA) and mercaptohexadecanoic acid (MHA), with a spacer length of 3, 11 and 16 carbon atoms, respectively, between the COOH and SH groups. To the functionalization, 100 µL of 10 mM in ethanol of each ligand was added to 1 mL of gold nanoparticle solution for 100 h at 800 rpm at room temperature (25 °C). A sample without ligands was used to control and evaluate the non-covalent interactions with the protein. An overview of the binders used in this work is shown in Table 1. The modified nanoparticles were washed three times by centrifugation (16.873g, 20 min) and then resuspended in ultrapure water. The materials were characterized by UV–Vis, FTIR and RAMAN.

### Protein coupling (BSA)

For the bioconjugation assays, zero-length crosslinkers were used, which are reagents that promote the binding between two molecules, without forming an additional compound between the two systems (Lacerda et al. 2010). Among them, the carbodiimides are widely applying. The strategy adopted in this work involves the study of covalent attachment of proteins onto AuNP surface using 1-ethyl-3-(3-dimethylaminopropyl)-carbodiimide (EDC) and N-hydroxysuccinimide (NHS) widely known as the EDC/NHS protocol for coupling reactions of SAMs with biomolecules (Hermanson 2008; Bartczak and Kanaras 2011a, b). The bioconjugation was performed by optimizing the method using EDC/

**Table 1** Data of the thiol grouping linkers used as spacers for coupling reactions

Ligand (spacer)	Abbreviation	Chemical structure	Molecular formula	MM (g/mol)	Length <sup>a</sup>
No ligands	S/L	—	—	—	<b>0</b>
Mercaptopropanoic acid	MPA		HSC <sub>2</sub> H <sub>4</sub> COOH	106.14	<b>3</b>
Mercaptoundecanoic acid	MUA		HSC <sub>10</sub> H <sub>20</sub> COOH	218.36	<b>11</b>
Mercaptohexadecanoic acid	MHA		HSC <sub>15</sub> H <sub>30</sub> COOH	288.49	<b>16</b>

<sup>a</sup>The length of the binder was determined by the number of carbon atoms in the SH and terminal COOH groups

NHS. To adjust the best coupling condition, assays were performed with different concentrations using the following molar ratios (EDC:NHS), 1:0, 1:1, 1:1.5, 1:2, 1:3 and 1:4. Thus, 100  $\mu$ L of AuNPs with modified surface with (MPA, MUA and MHA), 100  $\mu$ L of EDC (aq.) was added for 30 min and then 100  $\mu$ L of an aqueous solution of NHS (aq.). The reaction was kept under stirring (150 rpm) for 30 min. After this time 100  $\mu$ L of the protein (BSA, 15 mM) was inserted into the system and allowed to react for 30 min. Bovine serum albumin was immobilized through its amino groups, forming an amide bond with previously activated carboxylic acid (EDC/NHS). After the required time elapsed (30 min), the unbound proteins were removed by centrifugation and dosed by fluorescence. The amount of protein bound was calculated by subtracting the initial concentration minus the free protein detected in the supernatant.

## Results and discussion

### Synthesis and characterization of AUNPs

Size-controlled AuNP solution obtained through citrate reduction was characterized by UV–Vis, TEM, XRD and ICP-MS. The growth of as-synthesized AuNPs was monitored by the UV–Vis spectroscopy due to characteristic surface plasmon resonance (SPR) band. The UV–Vis spectrum reveals a narrow band at 522 nm, indicating the presence of monodisperse AuNPs (Fig. 1a). TEM was used to characterize size, shape and monodispersity of AuNPs, revealing a quasi-spherical shape with 18 nm diameter (Fig. 1b, d). These AuNPs were characterized as monodisperse as well with predominant spherical shape by AR, which were 1069 (details in Supporting Information, S1). The crystalline nature of AuNPs was confirmed by XRD analysis. The four intense diffraction peaks were observed at 2°, and the values found were 38.31°, 44.45°, 64.64° and 77.73°, corresponding to (111), (200), (220), And (311) reflection of the crystalline metallic gold, respectively. A strong diffraction peak (111) suggests that this pattern is the predominant

orientation of AuNPs (Fig. 1c). The concentration was determined by ICP-MS with 27.4 mg/L Au.

### AuNP surface analysis

AuNPs were stabilized by electrostatic repulsion of the negatively charged carboxylic ions of citrate adsorbed on their surface. Linkers with a stronger binding affinity, such as thiols (Lin et al. 2004; Briñas et al. 2013), can easily replace the citrate. Thus, in a second step, the mercaptocarboxylic linkers (MPA, MUA and MHA) replaced the citrate molecules. These ligands give access to new functionalization measures. One end (SH) binds to the surface and gives stability to the AuNPs while the other end (COOH) is exposed to the solution. Hence, the transfer constructs high affinity bonds between Au and S. On the other hand, free carboxylic acid may serve as an anchor for the other amine coupling reactions. In addition, the long alkyl chain provides sufficient flexibility so that the active moiety can interact with the multivalent receptor (Gasiorek et al. 2015). Dative bonds involving thiol-gold grouping are show in the Fig. 2.

To emphasize the difference between SAM's in contrast with AuNPs-cit, comparative measurements have been accomplished using UV–Vis spectroscopy (Fig. 3). The specters for AuNPs-cit and AuNPs with MPA, MUA and MHA were, respectively, 522, 523.5, 525 and 527 nm. The bathochromic shifts of the initial SPR band suggest that MPA, MUA and MHA have been coupled onto AuNP surface. Moreover, the single and narrow SPR bands of all ligands indicating a monodisperse population.

The dependence of LSPR band displacement on the chain length has also been studied. The regression analysis evidences the effect of the monolayer thickness (local dielectric environment) and the Au–S chemisorptions in the LSPR (Fig. 3b). It is possible to verify that an LSPR shifts to red 0.3 nm for each carbon atom. Since the refractive index of all the pure binders used in this work shows low variation, a linear dependence on the chain length can be attributed to the increase in the monolayer thickness. The maximum wavelength ( $\lambda$ ) values for AuNPs, before and after modification,

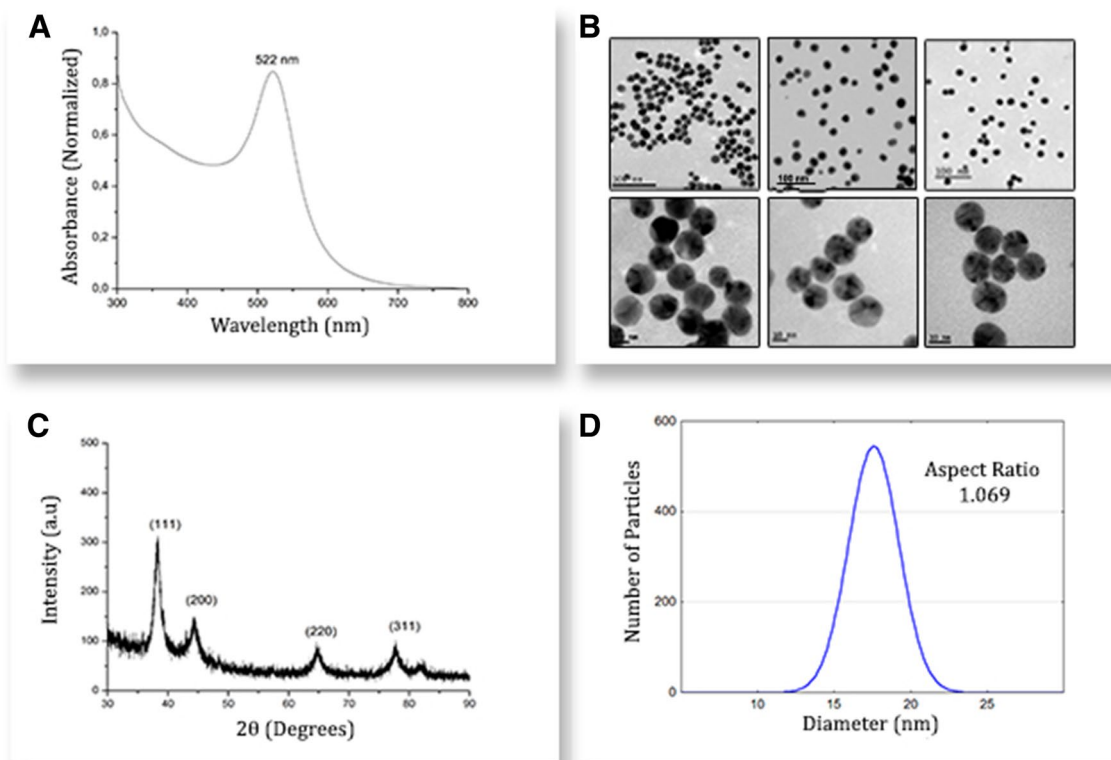


**Fig. 1** Characterization of AuNPs. UV–visible absorption spectroscopy for the gold colloid synthesized showing the characteristic plasmon peak at 522 nm (a); images obtained by transmission electron microscopy (b) at different magnifications showing the size and dis-

tribution of the synthesized nanoparticles. Scale bar 100 and 10 nm; X-ray diffraction pattern (c); histogram showing the Gaussian diameter distribution and the aspect ratio (AR) of 500 particles obtained by transmission electron microscopy images (d)

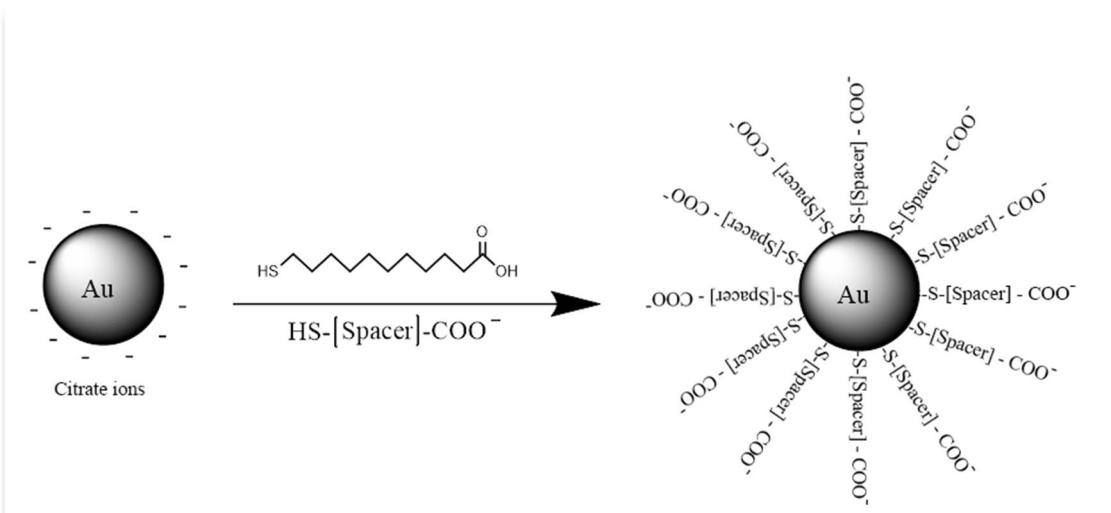


**Fig. 2** Representative scheme showing the functionalization of a gold nanoparticle with a mercaptocarboxylic linker, in this case mercaptoundecanoic acid with SH and COOH groups at each end

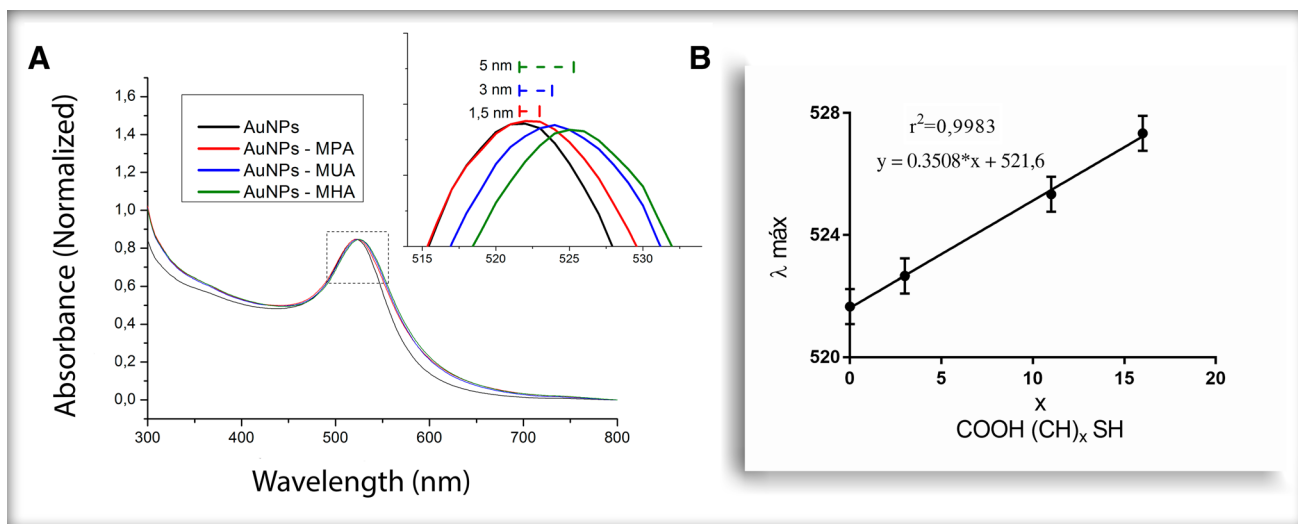


**Fig. 3** Mercaptopropanoic acid (MPA), mercaptoundecanoic acid (MUA) and mercaptohexadecanoic acid (MHA) functionalized AuNP absorption spectroscopy after 100 h of shaking (800 rpm) (a); chain length dependence in the spectral peak shift LSPR (b)

have been confirmed that the amount of carbon determines the displacement (Table 2). The linear dependence of the wavelength in relation to the thickness was also evidenced (Haes et al. 2004).

To confirm the successful and complete ligand exchange reaction, Fourier transform infrared (FTIR) spectroscopy (Fig. 4a) was carried out. Functional groups of as-synthesized MPA, MUA and MHA-capped AuNPs and their controls were identified by comparing the spectra. The presence of organic molecules onto AuNP surface was confirmed. The vibration peaks are observed in the region extending from the C–H group around  $2900\text{ cm}^{-1}$  for the MUA and MHA ligands. This spectrum shows peaks at  $2910$  and  $2840\text{ cm}^{-1}$  which are characteristics of the presence of asymmetric and symmetrical –CH stretching vibrations. These vibrations are associated with the carbon chain introduced by the functionalization onto AuNP surface with the ligands (Feng et al. 2015). In the MPA, a band is verified around  $1390\text{ cm}^{-1}$ , which is attributed to the axial deformation of the aliphatic C–H groups, as previously reported by (Roeges 1995). Bands around  $1600\text{ cm}^{-1}$  are characteristics of stretch flexural vibrations

of the hydroxyl group (Roeges 1995; Lin Vien et al. 1991; Socrates 1994). The displacements found around these absorption bands may be indicative of the coordination of the binder to the metal ion. The wide band found between  $3000$  and  $3400\text{ cm}^{-1}$  is related to the O–H stretching vibrations (Stuart 1997), which can be attributed to the presence of water due to the incomplete dehydration.

Raman spectroscopy was used to provide information about surface composition of as-synthesized AuNPs. The SERS effect of AuNPs-cit and MPA, MUA and MHA-capped AuNPs was studied (Fig. 4b). The Raman spectrum of the control (AuNPs-cit) showed broad bands at  $1358$  and  $1571\text{ cm}^{-1}$ , related to the carboxylic groups. Refer to asymmetric and symmetrical stretching vibrations ( $\text{COO}^{-1}$ ), respectively (Mak et al. 2013). The first peak is missing in the spectrum of AuNPs exposed to thiolated ligands, suggesting that the sulfide ions replaced part of the citrate ions chain. A peak around  $1106\text{ cm}^{-1}$  in the Raman spectrum of functionalized AuNPs is also observed, which may indicate the presence of S–C bonds (Prado et al. 2015), which are visible due to surface amplified Raman scattering (SERS).

**Table 2** Absorption wavelength shift data of alkaline-modified AuNPs (SAMs) of various chain types

Abbreviation	Ligand (spacer)	$C_x$	Before modification	After modification	$\Delta\lambda_{\text{max}}$ (nm)
AuNP's	No ligands	C0	522	522	0
AuNP's-MPA	Mercaptopropanoic acid	C3	522	523	1
AuNP's-MUA	Mercaptoundecanoic acid	C11	522	525	3
AuNP's-MHA	Mercaptohexadecanoic acid	C16	522	527	5



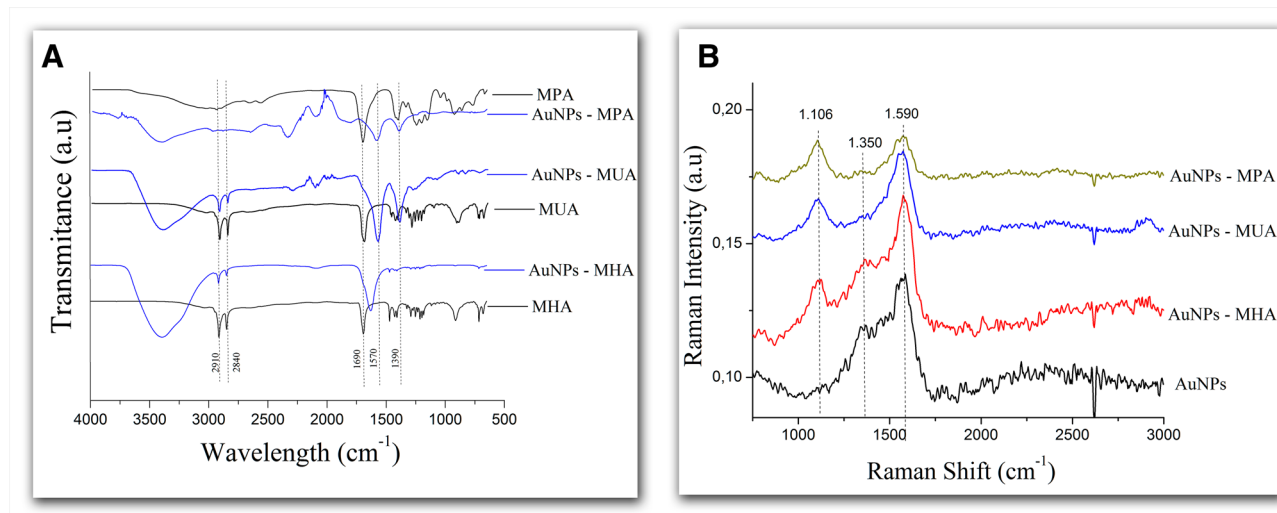


**Fig. 4** Infrared spectrum of metal nanoparticles functionalized with the binders after 100 h of stirring (800 rpm). In the black color, the ligand is shown as control and in the blue color is the spectrum of the AuNPs after the functionalization. *MPA* mercapropoanoic acid; *MUA* mercaptoundecanoic acid and *MHA* mercaptohexadecanoic

acid (a); Raman spectra and ligands of AuNPs after 100 h of stirring (800 rpm) and room temperature (25 °C). AuNPs control without ligands (black). AuNPs-MPA (red); AuNPs-MUA (blue) and AuNPs-MHA (green) (b)

### Stability of gold nanoparticles with modified surface

AuNPs prepared with sodium citrate are relatively stable and monodispersed. The citrate prevents aggregation due to negative surface charges. However, after the SAMs with terminal carboxylic acid onto AuNPs, it has been speculated that the complex becomes more vulnerable to particle aggregation and the destabilization strongly depends on the pH of the medium (Aslan and Pérez-Luna 2002). Thus, the stability of capped AuNPs needs to be monitored. Therefore, the stability of all AuNPs discussed here was studied in different pHs (3.0, 5.0, 7.0, 9.0, 10.0) and NaCl concentrations (0.25, 0.5, 1.0, 2.5, 5.0 and 10 mM) using UV–Vis spectroscopy (Fig. 5). Aggregated AuNPs tend to have a broader LSPR bands, with a red shift of  $\lambda_{\max}$  (Mulvaney 1996; Weisbecker et al. 1996; Mayya et al. 1997). Moreover, the flocculation assay was performed as a semi-quantitative aggregation measurement (Supporting Information, Fig. S2).

The flocculation parameter was calculated as a pH function (Fig. 5a–e). For all assays without binders, AuNPs were stable at neutral, alkaline and slightly acid pH ( $\text{pH} > 5$ ). The capped AuNPs tend to the same, except for the MPA that remained stable throughout the evaluated pH range (3–10), as evidenced by the flocculation assay. The instability presented by the other binders at  $\text{pH} < 5$  can be related to  $\text{pK}_a$  4.0 of the terminal carboxylic acid, so the electrostatic repulsion between particles is reduced in this pH range (Tandford 1962).

To be useful, AuNPs should exhibit stability not only over a wide pH range, but also over different ionic strength conditions (Lévy et al. 2004). Therefore, AuNPs with the modified surface were submitted to different concentrations of NaCl and had their absorption spectrum evaluated to investigate the influence of the ligand length as a function of ionic strength (Fig. 5e–i). AuNPs-cit was stable up to 10 mM at pH 7, without shifts in their absorption spectrum. NaCl-induced aggregation occurs from 5 mM for the capped AuNPs and is more pronounced at 10 mM, as can be seen the absorbance decrease from 522 nm and increase at longer wavelengths. The flocculation assay was also measured and the ligand length affects the colloidal stability. For the MPA, the aggregation parameter increases from 2.5 mM NaCl, which can be attributed to the MUA which showed a similar flocculation profile. AuNPs with the greater amount of carbons (MHA) showed good stability and low aggregation at the highest NaCl concentration (10 mM). In general, these results suggest a direct correlation between the ligand length and the stability of the modified surface nanoparticles. Other authors (Lévy et al. 2004) reported a direct influence of peptide chain size on the stability of AuNPs in different ionic strength conditions.

### Coupling reaction via EDC/NHS

The coupling efficiency using EDC/NHS is usually low and sensitive to pH variations. In addition, colloidal stability depends on a delicate balance between attraction and repulsion. Thus, coupling protocols require an optimization so as

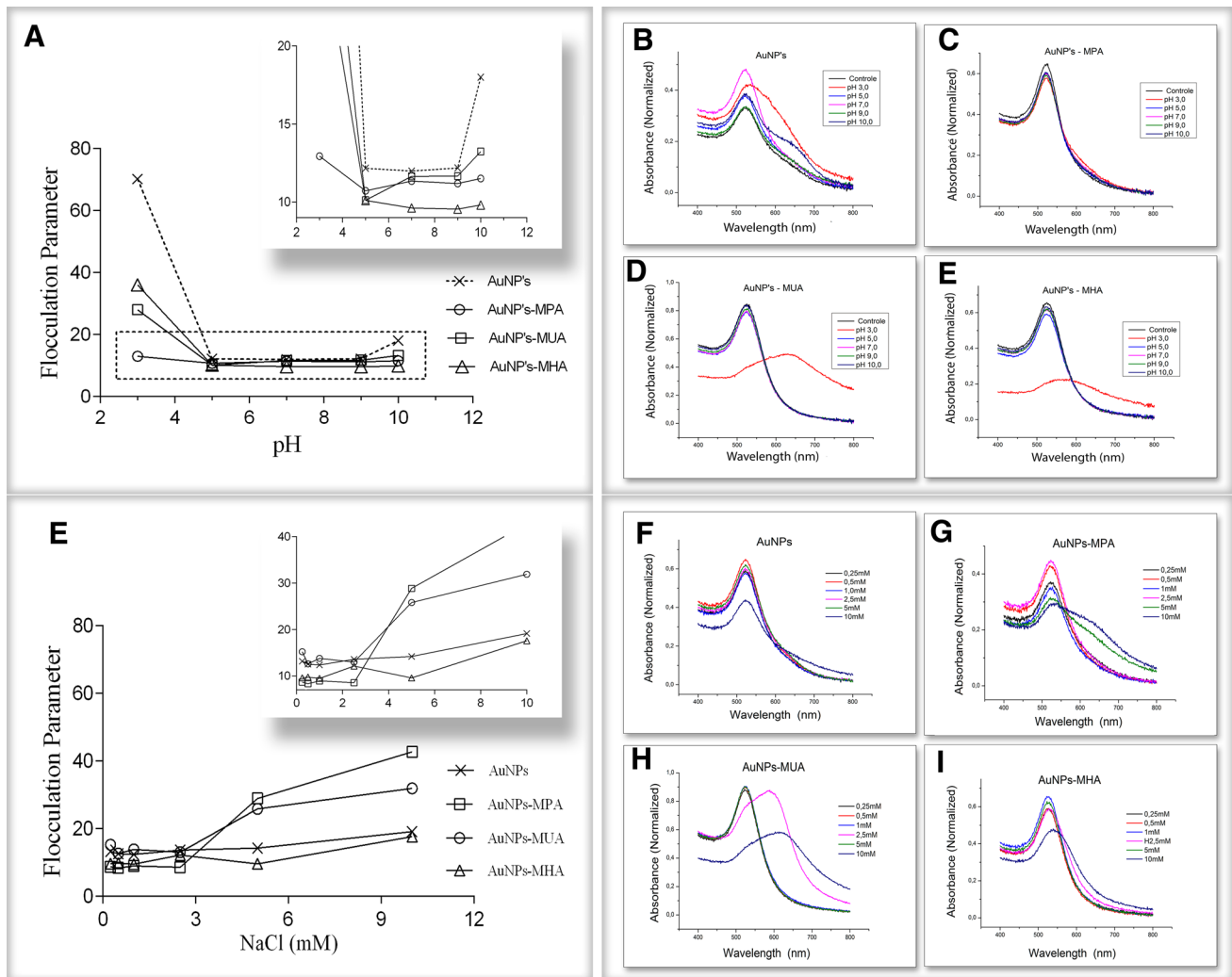


**Fig. 5** Flocculation parameter in relation to pH of colloidal gold with different binders (a); absorption spectrum showing the gold colloid with the binders at different pH ranges (3.0, 5.0, 7.0, 9.0, 10.0) and the control (no change in pH of the medium). AuNPs without binders (b); AuNPs functionalized with mercaptopropanoic acid (MPA) (c); AuNPs functionalized with mercaptoundecanoic acid (MUA) (d); AuNPs functionalized with mercaptohexadecanoic acid (MHA) (e); flocculation parameter in relation to the concentration of salts in colloidal gold with different binders (e); absorption spectrum showing the gold colloid with the binders at different concentrations of NaCl (0.25, 0.5, 1.0, 2.5, 5.0 and 10 mM). AuNPs without binders (f); AuNPs functionalized with mercaptopropanoic acid (MPA) (g); AuNPs functionalized with mercaptoundecanoic acid (MUA) (h); AuNPs functionalized with mercaptohexadecanoic acid (MHA) (i)

not to lose stability and achieve efficiency. The optimal reaction conditions may vary according to composition, size and shape of the metal and consequently their stability. Many authors have reported different concentrations of EDC/NHS for biomolecule coupling (Hermanson 2008; Bartczak and Kanaras 2011a, b; Jazayeri et al. 2016; Li et al. 2015).

In this work, we investigated the optimal molar ratio to conjugation of proteins using bovine serum protein (BSA). The intermediate chain binder (MUA) was used as standard and the quantification of total proteins was performed by fluorescence (Supporting Information, Fig. S3).

The total protein ratio as a function of variations of EDC/NHS molar ratio for BSA bioconjugation is presented

in Fig. 6. The reaction without the use of the stabilizing group (NHS) was also performed (EDC/NHS molar ratio 1:0). The optimum molar ratio for this assay was 1:1.5 (EDC/NHS). There was a decrease in conjugation efficiency with excess amount of the leaving group (NHS), which may be due to competition with the protein by the COOH groups activated with EDC (Supporting Information, Fig. S4).

After coupling, the bioconjugation was performed with all the spacers (MPA, MUA and MHA) and AuNPs as a control by electrostatic interaction. Total proteins ( $\mu\text{M}$ ) present onto AuNPs surface increase according the linker length (Fig. 6).

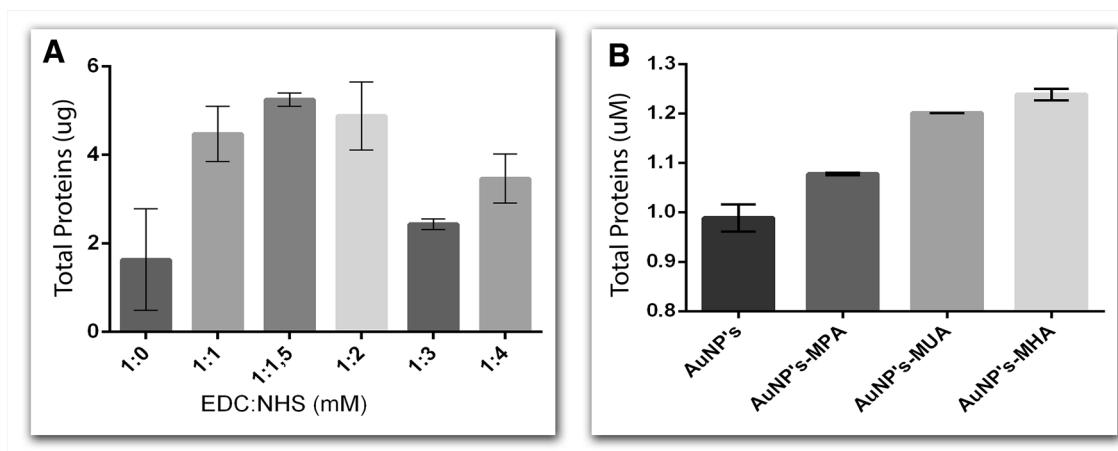


**Fig. 6** Effect of the molar ratio between the carboxylic acid activator (EDC) and the NHS (stabilizer) on the coupling of proteins on the surface of gold metallic nanoparticles (a); influence of spacer length on immobilization and proteins (BSA). *MPA* mercaptopropionic acid,

spacer length: 3 carbon atoms; mercaptoundecanoic acid (MUA), spacer length: 11 carbon atoms; *MHA* mercaptohexadecanoic acid, spacer length: 16 carbon atoms (b)

## Conclusions

In this study, we evaluated the use of mercaptocarboxylic binders of different lengths and discussed from their functionalization using standard techniques such as UV–Vis, IR, Raman, DLS, zeta potential and TEM. A study on the stability in different ranges of pH and ionic strength was carried out to identify the ideal working condition. The lowest binder evaluated (MPA) showed stability in a wide range of pH (3–10), however, the stability related to ionic strength was better for the long chain linker (MHA). Finally, an optimization using the EDC/NHS intermediates was performed for conjugation with biomolecules using bovine serum protein (BSA) as a template. The data presented show the influence of chain length on the covalent and non-covalent coupling steps with nanomaterials. Our results open new perspectives to understand the thickness influence of monolayers on the generation of reproducible and stable nanobioconjugates.

**Acknowledgements** The authors acknowledge financial support from the Brazilian Ministry of Science and Technology (CNPq Grant 483036/2011-0), the Ministry of Science and Technology (MCTI/FINEP/CT-INFRA grant PROINFRA 01/2006) and the Foundation Support Research and Innovation of Espírito Santo (Grant 006/2014). This work used the equipment facilities at the Laboratory of Cellular Ultrastructure Carlos Alberto Redins and the Laboratory of Biomolecular Analysis (LABIOM) at the Federal University of Espírito Santo, with thanks for providing the equipment and technical support for experiments.

**Author contributions** JPO conceived the project. JPO, ARP and WJK performed the characterizations and analysis. All authors contributed to discussions and writing of the manuscript. MCCG guided the research.

## References

- Arruebo M, Valladares M, Gonzalez-Fernandez A (2009) Antibody-conjugated nanoparticles for biomedical applications. *J Nanomater*. <https://doi.org/10.1155/2009/439389>
- Aslan K, Pérez-Luna VH (2002) Surface modification of colloidal gold by chemisorption of alkanethiols in the presence of a nonionic surfactant. *Langmuir* 18(16):6059–6065. <https://doi.org/10.1021/la025795x>
- Bartczak D, Kanaras A (2011a) Preparation of peptide-functionalized gold nanoparticles using one pot EDC/Sulfo-NHS coupling. *Langmuir* 27:10119–10123
- Bartczak D, Kanaras A (2011b) Preparation of peptide-functionalized gold nanoparticles using one pot EDC/sulfo-NHS coupling. *Langmuir* 27(16):10119–10123. <https://doi.org/10.1021/la2022177>
- Briñas RP, Maetani M, Barchi JJ (2013) A survey of place-exchange reaction for the preparation of water-soluble gold nanoparticles. *J Colloid Interface Sci* 392:415–421. <https://doi.org/10.1016/j.jcis.2012.06.042>
- El-Sayed MA (2004) Small is different: shape-, size-, and composition-dependent properties of some colloidal semiconductor nanocrystals. *Acc Chem Res* 37(5):326–333. <https://doi.org/10.1021/ar020204f>
- Feng AL, You ML, Tian L, Singamaneni S, Liu M, Duan Z, Lu TJ, Xu F, Lin M (2015) Distance-dependent plasmon-enhanced fluorescence of upconversion nanoparticles using polyelectrolyte multilayers as tunable spacers. *Sci Rep* 5:1–10. <https://doi.org/10.1038/srep07779>
- Gasiorek F, Pouokam E, Diener M, Schlecht S, Wickleder MS (2015) Effects of multivalent histamine supported on gold nanoparticles: activation of histamine receptors by derivatized histamine at subnanomolar concentrations. *Org Biomol Chem* 13(39):9984–9992. <https://doi.org/10.1039/C5OB01354B>
- Gole A, Murphy CJ (2008) Azide-derivatized gold nanorods: Functional materials for “Click” chemistry. *Langmuir* 24(1):266–272. <https://doi.org/10.1021/la7026303>
- Haes AJ, Zou S, Schatz GC, Van Duyne RP (2004) A nanoscale optical biosensor: the long range distance dependence of the



- localized surface plasmon resonance of noble metal nanoparticles. *J Phys Chem B* 108(1):109–116. <https://doi.org/10.1021/jp0361327>
- Hermanson GT (1996) *Bioconjugate techniques*. Academic Press, New York
- Hermanson GT (2008) *Bioconjugate techniques*, 2nd edn. Academic Press, San Diego
- Jain PK, El-Sayed IH, El-Sayed MA (2007) Au nanoparticles target cancer. *Nano Today* 2(1):18–29. [https://doi.org/10.1016/S1748-0132\(07\)70016-6](https://doi.org/10.1016/S1748-0132(07)70016-6)
- Jazayeri MH, Amani H, Pourfatollah AA, Pazoki-Toroudi H, Sedighmoghaddam B (2016) Various methods of gold nanoparticles (GNPs) conjugation to antibodies. *Sensing Bio Sensing Res* 9:17–22. <https://doi.org/10.1016/j.sbsr.2016.04.002>
- Kumar S, Aaron J, Sokolov K (2008) Directional conjugation of antibodies to nanoparticles for synthesis of multiplexed optical contrast agents with both delivery and targeting moieties. *Nat Protoc* 3:314–320. <https://doi.org/10.1038/nprot.2008.1>
- Lacerda SHD, Park JJ, Meuse C, Pristiniski D, Becker ML, Karim A, Douglas JF (2010) Interaction of gold nanoparticles with common human blood proteins. *ACS Nano* 4(1):365–379. <https://doi.org/10.1021/nn9011187>
- Levy R, Wang ZX, Duchesne L, Doty RC, Cooper AI, Brust M, Fernig DG (2006) A generic approach to monofunctionalized protein-like gold nanoparticles based on immobilized metal ion affinity chromatography. *ChemBiochem* 7(4):592–594. <https://doi.org/10.1002/cbic.200500457>
- Lévy R, Thanh NT, Doty RC, Hussain I, Nichols RJ, Schiffrin DJ, Brust M, Fernig DG (2004) Rational and combinatorial design of peptide capping ligands for gold nanoparticles. *J Am Chem Soc* 126(32):10076–10084. <https://doi.org/10.1021/ja0487269>
- Li CH, Kuo TR, Su HJ, Lai WY, Yang PC, Chen JS, Wang DY, Wu YC, Chen CC (2015) Fluorescence-guided probes of aptamer-targeted gold nanoparticles with computed tomography imaging accesses for in vivo tumor resection. *Sci Rep*. <https://doi.org/10.1038/srep15675>
- Lin S-Y, Tsai Y-T, Chen C-C, Lin C-M (2004) C.-H. Chen. Two-step functionalization of neutral and positively charged thiols onto citrate-stabilized Au nanoparticles. *J Phys Chem B* 108(7):2134–2139. <https://doi.org/10.1021/jp036310w>
- Lin Vien D, Colthup NB, Fateley WG, Graselli JG (1991) *The handbook of infrared and Raman characteristic frequencies of organic molecules*, 1st edn. Academic Press, San Diego
- Lynch I, Dawson KA Protein-nanoparticle interactions. *Nano Today* 2008, 3(1–2):40–47. [https://doi.org/10.1016/S1748-0132\(08\)70014-8](https://doi.org/10.1016/S1748-0132(08)70014-8)
- MacCuspie RI, Allen AJ, Hackley VA (2011) Dispersion stabilization of silver nanoparticles in synthetic lung fluid studied under in situ conditions. *Nanotoxicology* 5(2):140–156. <https://doi.org/10.3109/17435390.2010.504311>
- Mak JSW, Rutledge SA, Abu-Ghazal RM, Eftekhari F, Irizar TNCM, Zheng G, Helmy AS (2013) Recent developments in optofluidic-assisted Raman spectroscopy. *Prog Quantum Electron* 37(1):1–50. <https://doi.org/10.1016/j.pquantelec.2012.11.001>
- Mayya KS, Patil V, Sastry M (1997) On the stability of carboxylic acid derivatized gold colloidal particles: the role of colloidal solution pH studied by optical absorption spectroscopy. *Langmuir* 13(15):3944–3947. <https://doi.org/10.1021/la962140l>
- Mulvaney P (1996) Surface plasmon spectroscopy of nanosized metal particles. *Langmuir* 12(3):788–800. <https://doi.org/10.1021/la9502711>
- Oliveira JP, Prado AR, Keijok WJ, Pontes MJ, Ribeiro MRN, Nogueira BV, Guimarães MCC (2017) *Arab J Chem*. <https://doi.org/10.1016/j.arabjc.2017.04.003>
- Pease LF, Tsai DH, Zangmeister RA, Zachariah MR, Tarlov MJ (2007) Quantifying the surface coverage of conjugate molecules on functionalized nanoparticles. *J Phys Chem C* 111(46):17155–17157. <https://doi.org/10.1021/jp075571t>
- Peng G, Tisch U, Adams O, Hakim M, Shehada N, Broza YY, Bilan S, Abdah-Bortnyak R, Kuten A, Haick H (2009) Diagnosing lung cancer in exhaled breath using gold nanoparticles. *Nat Nanotechnol* 4(10):669–673. <https://doi.org/10.1038/nnano.2009.235>
- Prado AR, Oliveira JP, Pereira RH, Guimarães MC, Nogueira BV, Castro EV, Almeida LC, Ribeiro MR, Pontes MJ (2015) Surface-enhanced Raman plasmon in self-assembled sulfide-coated gold nanoparticle arrays. *Plasmonics* 10(5):1097–1103. <https://doi.org/10.1007/s11468-015-9909-2>
- Roeges PG (1995) A guide to the complete interpretation of infrared spectra of organic structures. *J Chem Educ* 72(4):A93. <https://doi.org/10.1021/ed072pA93.4>
- Saha K, Agasti SS, Kim C, Li X, Rotello VM (2012) Gold nanoparticles in chemical and biological sensing. *Chem Rev* 112(5):2739–2779. <https://doi.org/10.1021/cr2001178>
- Schroeder A, Heller DA, Winslow MM, Dahlman JE, Pratt GW, Langer R, Jacks T, Anderson DG (2012) Treating metastatic cancer with nanotechnology. *Nat Rev Cancer* 12(1):39–50. <https://doi.org/10.1038/nrc3180>
- Silvia F, Sally P, David AR, Kim ES (2000) Self-assembled monolayers: a versatile tool for the formulation of the biosurfaces. *Trends Anal Chem* 19(9):530–540. [https://doi.org/10.1016/S0165-9936\(00\)00032-7](https://doi.org/10.1016/S0165-9936(00)00032-7)
- Socrates G (1994) *Infrared characteristic group frequencies*, 2nd edn. Wiley, New York
- Sperling RA, Rivera-Gil P, Zhang F, Zanella M, Parak WJ (2008) Biological applications of gold nanoparticles. *Chem Soc Rev* 37(9):1896–1908. <https://doi.org/10.1039/b712170a>
- Stuart B (1997) *Biological applications of infrared spectroscopy*. ACOL Series, Wiley, Chichester
- Stuchinskaya T, Moreno M, Cook MJ, Edwards DR, Russell DA (2011) Targeted photodynamic therapy of breast cancer cells using antibody-phthalocyanine-gold nanoparticle conjugates. *Photochem Photobiol Sci* 10(5):822–831. <https://doi.org/10.1039/c1pp05014a>
- Sukhanova A, Even-Desrumeaux K, Kisserli A, Tabary T, Reveil B, Millot JM, Chames P, Baty D, Artemyev M, Oleinikov V, Pluot M, Cohen JHM, Nabiev I (2012) Oriented conjugates of single-domain antibodies and quantum dots: toward new generation of ultra-small diagnostic nanoprobe. *Nanomedicine* 8(4):516–525. <https://doi.org/10.1016/j.nano.2011.07.007>
- Tandford C (1962) The interpretation of hydrogen ion titration curves of proteins. *Adv Protein Chem* 17:69–165. [https://doi.org/10.1016/S0065-3233\(08\)60052-2](https://doi.org/10.1016/S0065-3233(08)60052-2)
- Terentyuk GS, Maslyakova GN, Suleymanova LV, Khlebtsov NG, Khlebtsov BN, Akchurin GG, Maksimova IL, Tuchin VV (2009) Laser-induced tissue hyperthermia mediated by gold nanoparticles: toward cancer phototherapy. *J Biomed Opt* 14(2):1–9. <https://doi.org/10.1117/1.3122371>
- Thobhani S, Attree S, Boyd R, Kumarswami N, Noble J, Szymanski M, Porter RA (2010) Bioconjugation and characterisation of gold colloid-labelled proteins. *J Immunol Methods* 356(1–2):60–69. <https://doi.org/10.1016/j.jim.2010.02.007>
- Tsai DH, Zangmeister RA, Pease LF, Tarlov MJ, Zachariah MR (2008) Gas-phase ion-mobility characterization of SAM-functionalized Au nanoparticles. *Langmuir* 24(16):8483–8490. <https://doi.org/10.1021/la7024846>
- Weisbecker CS, Merritt MV, Whitesides GM (1996) Molecular self-assembly of aliphatic thiols on gold colloids. *Langmuir* 12(16):3763–3772. <https://doi.org/10.1021/la950776r>
- Wilson R, Chen Y, Aveyard J (2004) One molecule per particle method for functionalising nanoparticles. *Chem Commun* 10:1156–1157. <https://doi.org/10.1039/B402786H>
- Zargar B, Hatamie A (2013) A simple and fast colorimetric method for detection of hydrazine in water samples based on formation

of gold nanoparticles as a colorimetric probe. *Sens Actuators B* 182:706–710. <https://doi.org/10.1016/j.snb.2013.03.036>

Zhou Y, Dong H, Liu L, Li M, Xiao K, Xu M (2014) Selective and sensitive colorimetric sensor of mercury (II) based on gold nanoparticles and 4-mercaptophenylboronic acid. *Sens Actuators B* 196:106–111. <https://doi.org/10.1016/j.snb.2014.01.060>

**Publisher's Note** Springer Nature remains neutral with regard to jurisdictional claims in published maps and institutional affiliations.